



# PtCo/rGO nano-anode catalyst: enhanced power density with reduced methanol crossover in direct methanol fuel cell

Richa Baronia<sup>1,2</sup> · Jyoti Goel<sup>2</sup> · Jyoti Kaswan<sup>1,2</sup> · Ajay Shukla<sup>1,2</sup> · Sunil K. Singhal<sup>2</sup> · Surinder P. Singh<sup>1,2</sup>

Received: 15 March 2018 / Accepted: 17 September 2018 / Published online: 22 September 2018  
© The Author(s) 2018

## Abstract

The higher methanol utilization efficiency in direct methanol fuel cell (DMFC) is one of the key factors that determine the performance of DMFC. Herein, we have synthesized bimetallic PtCo nano-particles (with optimized Pt:Co ratio) decorated reduced graphene oxide (rGO) nano-composite as anode catalyst. The electrochemical response of optimized PtCo (1:9)/rGO catalyst revealed efficient oxidation of 5 M methanol in half-cell configuration with ~60% Faradaic efficiency. A current density of 463.5 mA/cm<sup>2</sup> and a power density of 136.8 mW/cm<sup>2</sup> were achieved using PtCo (1:9)/rGO anode catalyst in a complete DMFC set-up at 100 °C with 5 M methanol supply which is ~three times greater as compared to commercial Pt/C (48.03 mW/cm<sup>2</sup>). The low activation energy of 9.88 kJ/mol indicates the faster methanol oxidation reduction (MOR) kinetics of PtCo (1:9)/rGO anode catalyst. Furthermore, the higher methanol utilization and open-circuit voltage in complete DMFC using PtCo (1:9)/rGO as compared to commercial Pt/C indicate the reduced methanol crossover. The excellent catalytic behavior of PtCo (1:9)/rGO towards MOR and high methanol utilization warrant its potential application as anode catalyst in DMFC.

**Keywords** PtCo nano-particles · Reduced graphene oxide (rGO) · Methanol oxidation · Fuel efficiency

## Introduction

Direct methanol fuel cells (DMFCs) are the promising source of green and affordable energy which directly converts chemical energy into electrical energy [1]. Methanol is considered as an attractive organic fuel due to its high power density (theoretical power density of 6100 Wh/kg at 25 °C, 30–40 times compared to Li-ion battery), low exhaust, and low operating temperatures [2, 3]. Despite its promises, DMFC suffers from sluggish reaction kinetics of methanol oxidation at the anode. Furthermore, the cell performance is considered to be adversely affected by the methanol

crossover, whereas the use of high methanol feed is considered advantageous for DMFCs. The reaction kinetics at the anode could be enhanced significantly by appropriate choice of catalyst that could reduce the initial activation over potential [4]. Conventionally, platinum supported on carbon has been used as an anode catalyst, but its activity degrades due to carbon monoxide (CO) poisoning and other carbonaceous species adsorption [5]. To overcome catalyst poisoning, Pt active sites could be regenerated by engineering the surface electronic and chemical properties via electronic structure manipulation through impregnation of transition metals (Co, Ni, Fe, Cr, V, and Ru), which will assist in dissociative adsorption of water molecules to form OH<sup>-</sup> species near Pt surface. These OH<sup>-</sup> species will promote the oxidation of CO on neighboring Pt sites and thereby facilitating its regeneration for further methanol oxidation reaction (MOR) [6].

Moreover, to attain maximum utilization efficiency and minimum platinum usage, the ultrafine Pt–M (M=Co, Ni, Cr, Pd, and Rh) alloys having large surface area with maximum active sites are proposed. However, the agglomeration and Ostwald's ripening of nano-particles may lead to deterioration in stability and activity of these alloys [7]. Recently, various engineered allotropes of carbon such as

**Electronic supplementary material** The online version of this article (<https://doi.org/10.1007/s40243-018-0134-8>) contains supplementary material, which is available to authorized users.

✉ Surinder P. Singh  
singhsp@nplindia.org

<sup>1</sup> AcSIR-Academy of Scientific and Innovative Research, CSIR-National Physical Laboratory Campus, New Delhi 110012, India

<sup>2</sup> CSIR-National Physical Laboratory, Dr. K. S. Krishnan Marg, New Delhi 110012, India

carbon black, carbon nanotubes, graphene, and graphene oxide (GO) have been investigated as a support matrix owing to their high surface area and a better electron conductivity [8]. The oxidized form of graphene, i.e., reduced graphene oxide (rGO) acts as a conductive material to modulate the electrochemical reaction in a controlled fashion. The presence of functional groups such as –OH and –COOH on rGO nanosheets provide sites for metal anchoring and their 2D structure allow higher loading of nanosize catalysts with almost no agglomeration contributing to higher current efficiency during MOR [9–11]. Furthermore, the hydrophilic nature of rGO promotes water activation at lower potential and induce the oxidation of adsorbed CO on active Pt sites of pure Pt or Pt–M nano-catalysts, by the bi-functional mechanism [12–14]. Among numerous reported bimetallic Pt-based catalysts, PtCo is considered a better catalyst as the incorporation of Co into the lattice of platinum introduce enhanced Pt d-band vacancies which modify the adsorption energy of the carbonaceous species on Pt surface and produce oxidized species at a lower potential [15, 16]. The modified electronic structure of PtCo alloys affects Pt–Pt bond distance resulting in easier adsorption of oxygen moieties on to alloy nano-particles and reduced CO poisoning [17]. Recently, we have reported the synthesis of PtCo nanoparticles with varying Pt and Co molar ratio onto rGO support using co-impregnation reduction method, where PtCo (1:9)/rGO catalyst showed the highest catalytic activity and long-term stability towards MOR [18].

In the present work, we have investigated the methanol oxidation efficiency and electrical performances of PtCo (1:9)/rGO catalyst at varying operating conditions and compared them with commercially available Pt/C catalyst. The detailed study of PtCo (1:9)/rGO electrocatalyst towards Faradaic efficiency, methanol utilization percentage, and activation energy for MOR have been carried out. The results for PtCo (1:9)/rGO catalyst show higher CO tolerance, resistance to methanol crossover, and high power density using 5 M methanol fuel feed (highest reported value to the best of our knowledge) indicating its commercial potential in DMFCs.

## Experimental

### Materials required

$\text{H}_2\text{PtCl}_6 \cdot 6\text{H}_2\text{O}$  (Alfa Aesar, 99.9%) and  $\text{CoCl}_2 \cdot 6\text{H}_2\text{O}$  (Alfa Aesar, 98%) were used as platinum and cobalt metal precursors, respectively, for the preparation of anode electrocatalysts.  $\text{NaNO}_3$  (Merck, Germany, > 98%),  $\text{KMnO}_4$  (Merck, Germany, > 98%),  $\text{H}_2\text{O}_2$  (Alfa Aesar, 30% in water),  $\text{NaOH}$  (Merck, Germany, > 98%), and  $(\text{CH}_2\text{OH})_2$  (Merck, Germany) were used to prepare the catalyst. Nafion<sup>®</sup> 117 (DE

521, DuPont, USA) dispersion was used to prepare catalyst slurry. Methanol ( $\text{CH}_3\text{OH}$ ) (Merck, Germany, > 98%) and sulfuric acid ( $\text{H}_2\text{SO}_4$ ) (Merck, Germany) were used as fuel and as electrolyte, respectively. Ultrahigh-purity graphite powder (Ultra Carbon, USA) was used for the synthesis of (GO). Commercially used Pt/C catalyst was procured from Alfa aesar. De-ionized (DI) water was used for all the experiments.

### Preparation of graphene oxide

Graphene oxide has been synthesized from graphite powder using modified Hummers method reported by Kovtyukhova et al. [19]. The pre-oxidized graphite powder (0.5 g) was treated with concentrated sulfuric acid (20 mL) at 0 °C. Then,  $\text{NaNO}_3$  (0.5 g) and  $\text{KMnO}_4$  (1.5 g) were added with continuous stirring. After keeping the mixture at room temperature for 3 h, the temperature was raised to 35 °C and stirred for 30 min. In the resulting mixture, DI water (100 mL) was added slowly and the temperature of the solution increased as result of the exothermic reaction. After bringing the solution to room temperature, 30%  $\text{H}_2\text{O}_2$  (1 mL) was added and centrifuged at 12,000 rpm till a pH value of 7 is attained. This GO powder was further used for the preparation of different compositions of PtCo/rGO electrocatalysts by the co-impregnation reduction method.

### Catalyst preparation

The PtCo (1:9)/rGO electrocatalyst has been prepared using co-impregnation reduction and the detailed method with optimization has been published elsewhere [18]. A calculated amount of graphene oxide, Pt, and Co metal precursors were first refluxed and stirred with ethylene glycol at 120 °C for 5 h and then ultrasonicated for 2 h. The resulting solution was washed, centrifuged, and vacuum dried to obtain the desired ratio of PtCo/rGO catalysts.

### Physical characterization

The structural properties of rGO and PtCo/rGO were studied by powder X-ray diffraction using Rigaku miniflex-300 bench top X-ray diffractometer having  $\text{Cu K}\alpha$  ( $\lambda = 1.541\text{\AA}$ ) X-ray source. The infrared spectra of synthesized support and catalyst were measured in ATR mode using Agilent Cary 360 Fourier transform infrared (FTIR) spectrometer. Raman measurements were conducted on Ranishaw win-via reflex spectrometer within the spectral range of 500–3000/cm. Atomic Force Microscope nanoscope (Veeco V) was used to identify the formation of single or few layers of graphene oxide by capturing topographical images in tapping mode. The morphology of rGO, commercial Pt/C and PtRu/C and PtCo/rGO anode catalysts and the dispersion

nano-particles onto reduced graphene oxide nanosheets was studied using transmission electron microscopy (TEM), Tecnai G2 F30 S-Twin (FEI; Super twin lens with  $C_s = 1.2$  mm) instrument operated at accelerating voltage of 300 kV, having a point resolution of 0.2 nm and lattice resolution of 0.14 nm. The morphology of rGO was also imaged using scanning electron microscopy (SEM), FEI, and Quanta FEG 450. X-ray photoelectron spectroscopy (XPS) measurements were performed using monochromatic AlK $\alpha$  X-ray source and EA 125 HR electron analyzer from Omicron GmbH. Core levels were acquired using 20 eV pass energy. Overall experimental resolution is about 0.4 eV and binding energy (BE) calibration of spectrometer is done using Fermi edge position of a clean polycrystalline silver foil. Shirley background subtraction was performed on each core level. Uncertainty in determining the BE position and full width at half maximum (FWHM) is estimated to be  $\pm 0.05$  eV. Uncertainty in determining relative percentage is estimated to be  $\pm 5\%$  of the base value.

### Electrochemical measurements

The electrochemical activity of commercial Pt/C and PtCo (1:9)/rGO catalyst has been evaluated using cyclic voltammetry in a standard three-electrode cell using electrochemical workstation (Palm Sens 3) at room temperature. Ag/AgCl was used as a reference electrode and Pt mesh as the counter electrode. Glassy carbon (GC) was used as the working electrode. For the preparation of working electrode, 2.5 mg of the catalyst was dispersed in 500  $\mu$ L of 5% Nafion<sup>®</sup> 117 dispersion and ultrasonicated for 1 h. 5  $\mu$ L of the dispersed electrocatalyst was drop cast onto the glassy carbon electrode surface and dried at room temperature for 1 h. Prior to drop cast, the electrodes were polished well with 0.05  $\mu$ m alumina pastes and washed with DI water. The methanol electrooxidation efficiency of PtCo (1:9)/rGO and commercially available Pt/C, electrocatalysts was evaluated using cyclic voltammetry (CV) curves in 1 M H<sub>2</sub>SO<sub>4</sub> and varying concentrations of CH<sub>3</sub>OH solution, i.e., 1–6 M at a scan rate of 20 mV/s in the voltage range of 0–1.0 V. Similar experiments were performed for chronoamperometric (CA) measurements to study the long-term stability of various catalysts. CA measurements were done at 0.7 V in CH<sub>3</sub>OH and H<sub>2</sub>SO<sub>4</sub> aqueous solution for 3600 s.

### Methanol oxidation reaction by-product estimation

The methanol electrooxidation reaction product analysis was carried out using UV–visible spectrophotometer (Agilent technologies, CARY 5000 series). To estimate methanol oxidation by-products (formic acid and formaldehyde), CA measurements were done at 0.7 V in varying concentrations of CH<sub>3</sub>OH and 1.0 M H<sub>2</sub>SO<sub>4</sub> in aqueous solution for 3600 s.

The resulting solution was subjected to spectroscopic analysis to measure optical density (OD) at 350 nm and 280 nm for formic acid and formaldehyde, respectively, corresponding to their concentrations. The UV–visible scans were done in the wavelength range from 200 to 500 nm to monitor respective ODs, by taking 3 mL of oxidized solution in a quartz cuvette (10 mm path length). For each distinctive peak related to the by-products, the standard curves were plotted.

### Direct methanol complete cell test

The performance of rGO-supported PtCo nano-catalysts synthesized in the present work was tested using single DMFC set-up. The membrane electrode assembly (MEA) was prepared using the conventional method [20]. The catalysts tested in the anode side were commercial Pt/C and PtCo (1:9)/rGO with 3 mg/cm<sup>2</sup> loading. Pt/C (40 wt.%) with 1 mg/cm<sup>2</sup> catalyst loading was used at the cathode side in all the tests. The catalyst slurry was prepared by mixing the calculated amount of catalyst with Nafion<sup>®</sup> 117 (DE 521, DuPont, USA) dispersion in an ultrasonic bath for 1 h. The prepared slurry was spread onto the porous carbon paper (90 T, Toray, USA) and dried at 100 °C for 1 h to develop the anode and cathode electrodes. Nafion<sup>®</sup> 117 membranes were treated with H<sub>2</sub>O<sub>2</sub> (3 wt.%) and 1 M H<sub>2</sub>SO<sub>4</sub> for 1 h each. The treated membrane was sandwiched between the catalyst-coated anode and cathode electrodes to obtain MEA. The current–voltage characteristics were obtained using potentiostat–galvanostat (Autolab, PGSTAT 30, GPES). Effect of variation in methanol fuel concentration and operating temperature was also studied using the same DMFC cell set-up.

## Results and discussion

The detailed physical characterization of highly exfoliated rGO sheets serving as support matrix for PtCo nano-particle catalyst was carried out using AFM, SEM, TEM, and Raman spectroscopy, and is given as supplementary information (Fig. S1a–d). Furthermore, the structural properties of synthesized PtCo (1:9)/rGO and commercial Pt/C catalyst have been investigated using XRD and TEM. Figure 1 shows the XRD pattern for commercial Pt/C and PtCo (1:9)/rGO nano-composite exhibiting the characteristic diffraction peaks at 39.54°, 45.90°, and 67.9° corresponding to the (111), (200), and (220) planes of the face-centered cubic (FCC) structure of Pt (JCPDS 87-0646). The right-hand shift in  $2\theta$  value for PtCo (1:9)/rGO as compared to Pt/C revealed a decrease in the ‘d’ spacing due to lattice contraction because of smaller Co atom substitution for Pt indicating the formation of PtCo alloy. The average metal particle size for Pt/C and PtCo

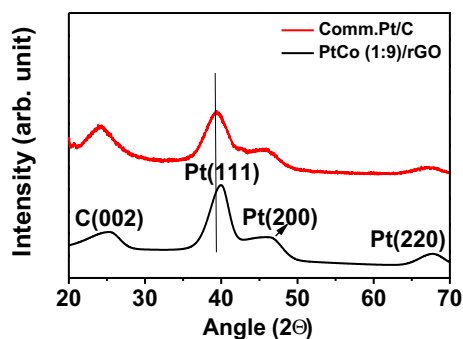


**Fig. 1** X-ray diffraction pattern of commercial Pt/C and PtCo (1:9)/rGO

(1:9)/rGO is observed to be 2–3 nm, whereas, for commercial PtRu/C, the metal particles size is ~ 18 nm as observed from TEM measurements shown in Fig. 2a–c. It could be clearly seen that PtCo nano-particles in PtCo (1:9)/rGO composite are uniformly and densely distributed onto rGO sheets compared to Pt and PtRu nano-particle on carbon support indicating higher loading of PtCo (1:9) on rGO sheets that would contribute to higher catalytic performance. The smaller size and dense distribution of PtCo nano-particles onto rGO sheets is attributed to the anchoring site provided by defects in rGO for metal ions during the synthesis process; both these parameters are critical in achieving improved activity and stability of the catalyst [21]. Figure S2a depicts FTIR spectra of rGO in which peaks at  $3171/\text{cm}^{-1}$ ,  $1583/\text{cm}^{-1}$ ,  $1218/\text{cm}^{-1}$ ,  $1226/\text{cm}^{-1}$ , and  $1068/\text{cm}^{-1}$  correspond to OH stretching of hydroxyl groups, C–O stretching of the carboxyl, epoxy, and alkoxy groups, respectively, revealing the hydrophilic nature of rGO sheets. However, the intensity of these peaks was reduced significantly when PtCo was decorated on to rGO sheets indicating deoxygenation of graphene oxide [22]. Figure S2b shows the Raman spectra of rGO and PtCo/rGO. The presence of D-band related to defects induced breathing mode at  $1354/\text{cm}^{-1}$  and the G-band related to

the  $\text{sp}^2$  carbon at  $1596/\text{cm}^{-1}$  confirms the formation of rGO. The D- and G-bands in PtCo/rGO nano-composite were observed at  $1361$  and  $1597/\text{cm}^{-1}$ . The  $I_{\text{D}}/I_{\text{G}}$  ratios for rGO and PtCo/rGO were calculated to be 0.88 and 0.98, respectively. The higher value of  $I_{\text{D}}/I_{\text{G}}$  ratio for PtCo/rGO suggests that overall defects have increased on loading of PtCo nano-particles onto rGO sheets [23].

Furthermore, XPS spectra exhibiting the characteristic features for rGO and PtCo over a selected binding energy (BE) range have been shown in (Fig. 3a, b). C 1s core-level spectra of rGO and PtCo(1:9)/rGO samples are compared in Fig. 3a. C 1s core levels have been fitted using five near Gaussian components which correspond to C=C/C–C, C–OH, C–O, C=O, and –COOH [24]. Attachment of PtCo(1:9) to rGO results in further reduction as C–O component of C 1s core level in PtCo(1:9)/rGO is significantly reduced compared to rGO sample. Figure 3b shows the Pt 4f core-level spectra for commercial Pt/C and PtCo(1:9)/rGO samples. Spin–orbit splitted components ( $4f_{7/2}$  and  $4f_{5/2}$ ) of Pt 4f core levels have been fitted using three peaks to achieve satisfactory fit. Full width at half maximum has been kept the same for fitting components corresponding to spin–orbit splitted peaks along with maintaining branching ratio of 4:3 and keeping spin–orbit splitting fixed. Fitting components for Pt  $4f_{7/2}$  of commercial Pt/C appear at 71.35, 72.05, and 73.95 eV, and these can be assigned to metallic Pt [Pt(0)] and higher valence states of Pt [Pt(II) and Pt(IV)], respectively [25–27]. For Pt  $4f_{7/2}$  of PtCo(1:9)/rGO, Pt(0)-, Pt(II)-, and Pt(IV)-related peaks appear at 71.55, 72.3, and 74.35 eV, respectively, and thus exhibit 0.2 eV positive BE shift compared to commercial Pt/C sample. Such shift has been seen in the cases of PtCo alloys and it has been associated with the loss of 5d electrons of Pt when alloyed with Co and also attributed to the increased interaction with oxygen atoms and resultant higher catalytic activity of PtCo alloy compared to pure Pt [13]. It is also interesting to note that relative percentage of higher valence states of Pt [Pt(0):Pt(II):Pt(IV) = 33.8:43.3:22.9] is more for PtCo(1:9)/

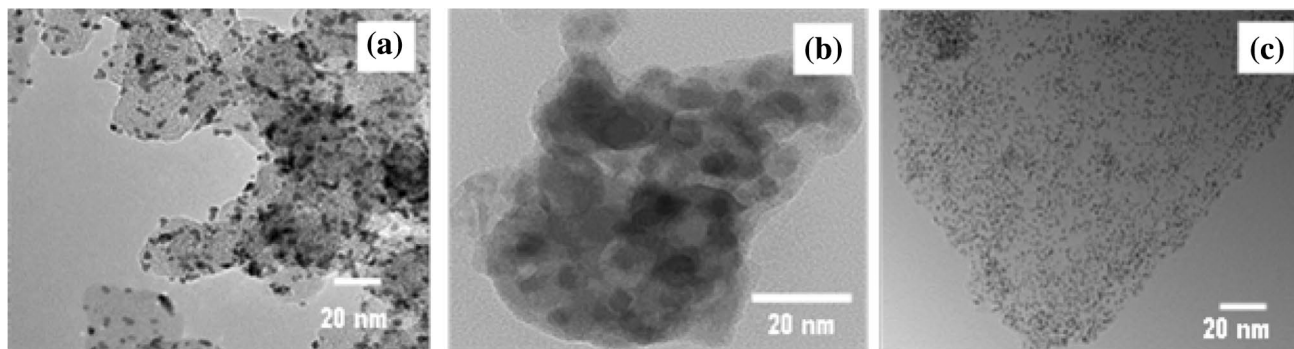


**Fig. 2** TEM micrographs of **a** comm. Pt/C **b** comm. PtRu/C **c** PtCo (1:9)/rGO

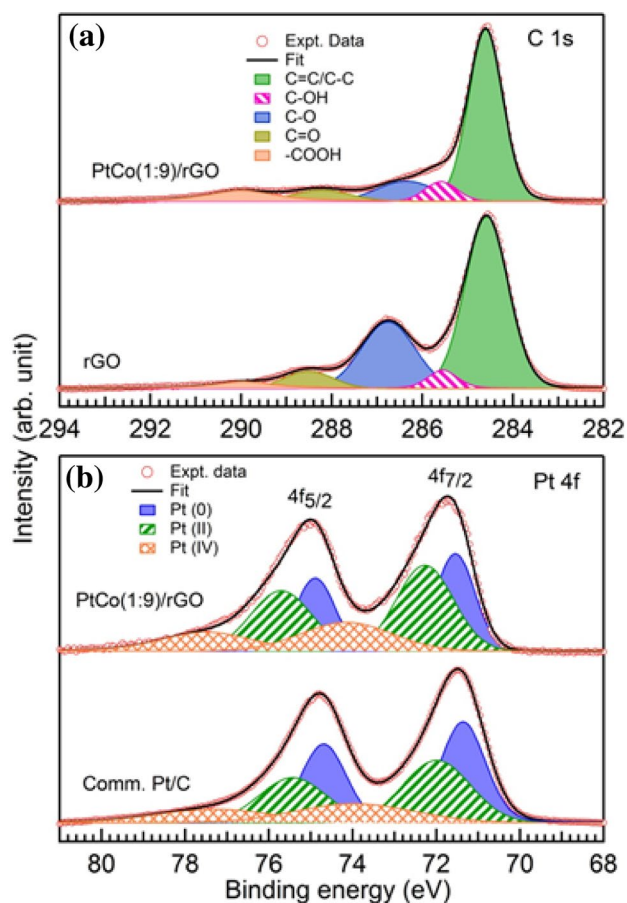


**Fig. 3** XPS core-level spectra. **a** C 1s core-level spectra (open circles) for rGO and PtCo(1:9)/rGO samples. **b** Pt 4f core-level spectra of commercial Pt/C and PtCo(1:9)/rGO samples. Fitted data (solid line) and deconvoluted fitting components (shaded and patterned regions) are also shown here

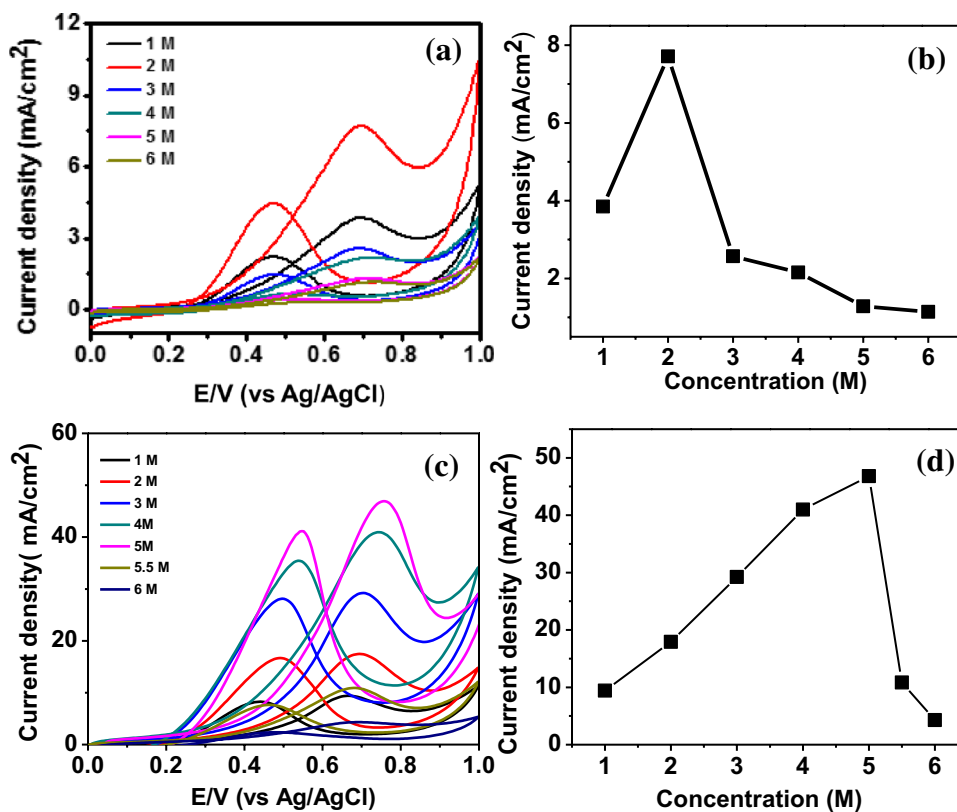
rGO compared to Pt/C [Pt(0):Pt(II):Pt(IV)] = 43.1:37.1:19.8] indicating the electronic structure modification of Pt and thereby expected to enhance the catalytic properties of PtCo(1:9)/rGO compared to Pt/C with more CO tolerance. XPS core-level data show that Co is in divalent state in the PtCo(1:9)/rGO (Fig. S3).

The CV has been used to evaluate the electrochemical properties and MOR efficiency of the synthesized PtCo (1:9)/rGO nano-composites, commercial Pt/C and PtRu/C. Figure 4a, c shows the MOR kinetics and Fig. 4b, d represents the dependence of forward oxidation peak current on the methanol concentration of Pt/C and PtCo (1:9)/rGO anode catalyst, respectively. The peak anodic current density for Pt/C is found to be 7.71 mA/cm<sup>2</sup> at 2 M methanol concentration, and thereafter, a continuous decrease is observed up to 6 M. Interestingly, the anodic peak current density for PtCo (1:9)/rGO increases from 9.38 to 46.8 mA/cm<sup>2</sup> for methanol concentration of 1–5 M and then decreases to about 4 mA/cm<sup>2</sup> on further increasing the methanol

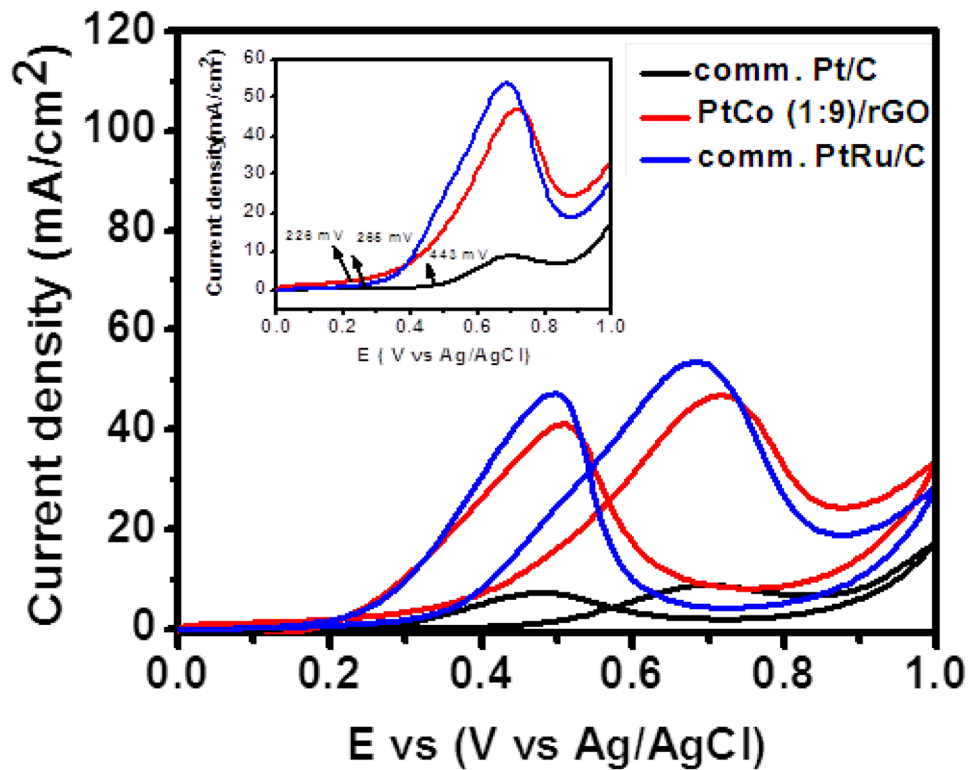
concentration to 6 M. It is worth noting that the PtCo (1:9)/rGO catalyst exhibits six times higher maximum peak current density at 5 M as compared to commercial Pt/C electrocatalyst at 2 M methanol concentration, indicating efficient MOR and higher methanol utilization. Furthermore, the decrease in current density at higher methanol concentration (above 5 M) is attributed to the saturation of electrode active site by methanol molecules and also contamination of catalyst surface by the intermediate products during the methanol oxidation [21]. In addition, MOR activity of highly efficient commercial PtRu/C anode catalyst is compared with PtCo(1:9)/rGO and commercial Pt/C. Figure 5 shows the CV curves representing catalytic activity of commercial Pt/C in 1 M H<sub>2</sub>SO<sub>4</sub> and 2 M CH<sub>3</sub>OH along-with commercial PtRu/C and PtCo (1:9)/rGO anode catalyst in the presence of 1 M H<sub>2</sub>SO<sub>4</sub> and 5 M CH<sub>3</sub>OH at a scan rate of 20 mV/s. The MOR onset potential of PtCo (1:9)/rGO anode catalyst is negatively shifted by ~200 mV and ~40 mV, as compared to commercial Pt/C and PtRu/C, respectively, and is shown in Fig. 5 (inset). The negatively shifted MOR onset potential indicates that the overpotential of methanol oxidation is lower and facilitates the fast methanol oxidation at the electrode surface [28]. The ratio of forward anodic peak current density related to methanol oxidation and backward peak current density corresponding to the removal of the incompletely oxidized carbonaceous species defines the carbon mono-oxide tolerance of the catalyst [16]. The  $I_F/I_B$  ratios for PtCo (1:9)/rGO, commercial PtRu/C, and Pt/C are 1.139, 1.133, and 1.264, respectively. The  $I_F/I_B$  ratio for the synthesized PtCo (1:9)/rGO catalysts similar to PtRu/C suggests comparable carbonaceous species tolerance.

The catalytic stability of commercial Pt/C (2 M CH<sub>3</sub>OH), PtRu/C (5 M CH<sub>3</sub>OH), and PtCo (1:9)/rGO (5 M CH<sub>3</sub>OH) catalysts were analyzed at 0.7 V for 3600 s using chronoamperometry technique. Figure 6 shows the chronoamperometric curves for PtCo (1:9)/rGO, commercial PtRu/C, and Pt/C electrocatalysts. A fast decay in the initial current density was observed for all the catalysts, which is attributed to the formation of surface adsorbed intermediate species, such as CO<sub>ads</sub>, CH<sub>3</sub>OH<sub>ads</sub>, and CHO<sub>ads</sub>, during the methanol oxidation reaction and is in agreement with the reported results [29]. The sub-linear decay in current density for PtCo(1:9)/rGO could be associated with the multifunctional adsorption and desorption kinetics of carbonaceous species. The methanol oxidation current for PtCo (1:9)/rGO catalysts reaches to stabilization at 5.206 mA/cm<sup>2</sup>, whereas, for commercial PtRu/C catalyst and Pt/C, it stabilizes at 1.681 mA/cm<sup>2</sup> and 0.21 mA/cm<sup>2</sup>, respectively. The ~four times higher residual current density for PtCo (1:9)/rGO compared to PtRu/C catalyst after 3600 s indicates the higher electrocatalytic activity, stability, and greater extent of CO tolerance. In case of smaller particles size, a higher fraction of surface atoms interact with carbon support compared to the larger

**Fig. 4** Cyclic voltamograms of **a** commercial Pt/C e PtCo (1:9)/rGO catalyst with varying methanol concentrations at a scan rate of 20 mV/s **b, d** show the corresponding methanol oxidation peak current vs methanol concentration plots



**Fig. 5** Cyclic voltamograms (CV) at a scan rate of 20 mV/s, commercial Pt/C in 1 M H<sub>2</sub>SO<sub>4</sub>+2 M CH<sub>3</sub>OH and commercial PtRu/C, PtCo (1:9)/rGO in 1 M H<sub>2</sub>SO<sub>4</sub>+5 M CH<sub>3</sub>OH, exhibiting maximum current density (inset shows the onset potential for both the catalysts)



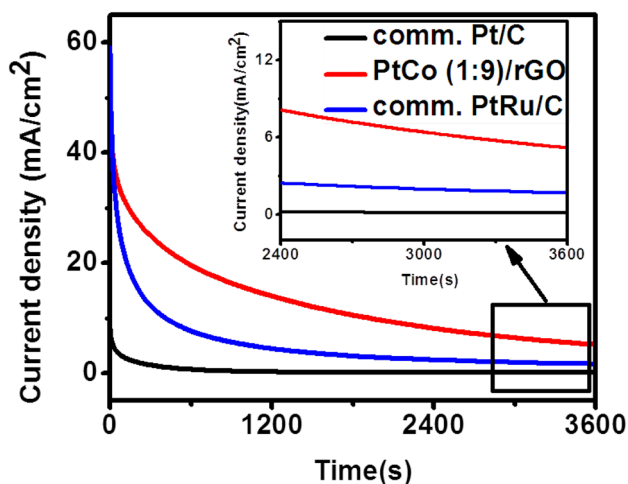


**Fig. 6** Chronoamperometric measurements for commercial Pt/C in 1 M H<sub>2</sub>SO<sub>4</sub>+2 M CH<sub>3</sub>OH and PtCo (1:9)/rGO in 1 M H<sub>2</sub>SO<sub>4</sub>+5 M CH<sub>3</sub>OH at 0.7 V for 3600 s

particles and improve the charge transfer and enhance the catalytic activity [30]. Furthermore, the hydrophilic nature of rGO promotes water activation and helps in oxidizing CO-adsorbed onto metallic catalyst surface; also strong interaction between Pt and rGO modulates favorably the Pt electronic structure [12]. The enhanced performance of PtCo (1:9)/rGO towards MOR could be attributed to densely distributed smaller size PtCo nano-particles onto the rGO nanosheets (Fig. 2c) and electronics structure modulation of PtCo on the surface of rGO corroborated by XPS measurements.

The long-term poisoning rate of a catalyst is calculated by measuring the linear decay of current using the following equation [7]:

$$\delta\left(\frac{\%}{s}\right) = \frac{100}{I_0} \times \left(\frac{dI}{dT}\right)_{t>500s}, \tag{1}$$

where  $(dI/dt)_{t>500s}$  is the slope of the linear portion of the current decay, and  $I_0$  is the residual current density

calculated by extrapolating linear current decay values from CA curves. According to the above equation, the poisoning rate of PtCo (1:9)/rGO is calculated to be 0.021% per s which is about 42% lower than previously reported using pure Pt nano-particles (0.05% per s) as the anode catalyst in DMFC [7]. The reduction in electrode poisoning rate for PtCo (1:9)/rGO indicates that this novel electrocatalyst has higher tolerance towards CO and other intermediate carbonaceous species that are responsible for degrading the electrode activity.

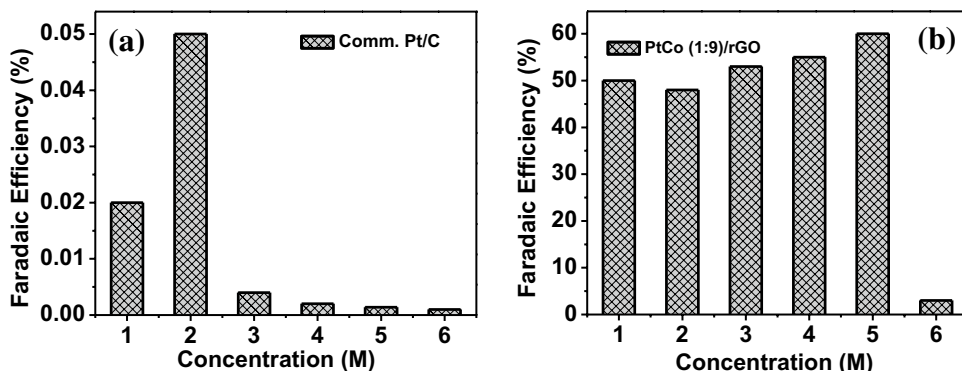
Faradaic efficiency ( $\eta$ ) of fuel cell in a half-cell configuration is used to investigate the fuel utilization capabilities of PtCo (1:9)/rGO catalyst and commercial Pt/C by varying the methanol concentrations and have been calculated using the following equations [31]:

$$\eta = \frac{\text{discharging capacity (Ah)}}{\text{theoretical discharging capacity (Ah)}}, \tag{2}$$

$$\eta = \frac{\int_0^t i(t)dt}{6C_M V_M F}, \tag{3}$$

where  $t$  is the time required in discharging,  $i(t)$  is the discharging current,  $C_M$  is methanol concentration,  $V_M$  is the volume of methanol solution, and  $F$  is Faraday constant (96485.33 C/mol). Figure 7a shows the Faradaic efficiency of commercial Pt/C with varying methanol concentrations from 1 to 6 M, which is highest (~0.05%) at 2 M methanol. On the other hand, the highest Faradaic efficiency of ~60% (Fig. 7b) was observed for PtCo (1:9)/rGO catalyst at 5 M methanol concentration. Interestingly, the faradic efficiency of PtCo (1:9)/rGO catalyst is ~46% at 2 M methanol concentration which is also way higher than that of commercial Pt/C. Furthermore, an abrupt decrease in Faradaic efficiency was observed from 60 to 6% for PtCo (1:9)/rGO as the methanol concentration was increased from 5 to 6 M; this is attributed to the saturation of active sites of the catalyst which were not further available for the oxidation process. Moreover, Liu et al. [31] have reported about 22% Faradaic efficiency

**Fig. 7** Faradaic efficiency of half-cell DMFC at different methanol concentrations for a commercial Pt/C b PtCo (1:9)/rGO



using passive DMFC in 5 M methanol concentration, which is significantly lower to that observed in the present work. This enhancement in Faradaic efficiency indicates lower methanol crossover up to 5 M methanol concentration and hence enhancement in the DMFC performance.

The turn over number (TON) for methanol oxidation in DMFC defines the number of methanol molecules that react per catalyst surface site per second and can be seen from steady-state current from CA measurements of methanol oxidation. The TON values were calculated using the following relation [32]:

$$\text{TON} \left[ \frac{\text{molecules}}{\text{sec. surface}} \right] = \frac{I [\text{mA/cm}^{-2}] \times N_A}{nF \times m (\text{Pt}) [\text{cm}^{-2}]}, \quad (4)$$

where,  $I$  is the steady-state current density measured experimentally using CA curves (presented in Fig. 6),  $N_A$  is the Avagadro's constant ( $6.023 \times 10^{23}$ ),  $n$  is the number of electrons produced in the oxidation of one methanol molecule and is assumed to be 6,  $F$  is the Faraday's constant ( $96485.33 \text{ }^\circ\text{C}$ ), and  $m$  is the mean atomic density ( $1.51 \times 10^{15}/\text{cm}^2$ ) of surface Pt atoms at (111) surface. The TON for methanol electrooxidation for PtCo (1:9)/rGO and Pt/C were found to be 6.0554/s and 0.1064/s, respectively. The higher TON, thereby enhanced the catalytic activity of PtCo (1:9)/rGO, is attributed to the synergy between PtCo and rGO nanosheets providing an increased number of catalytic sites/unit mass and fast electron transfer. The structural changes, in optimized PtCo (1:9)/rGO due to the specific composition of Co atoms, significantly affect the turnover number as the MOR is surface and structure-sensitive reactions [33]. The by-product formation from MOR on PtCo (1:9)/rGO and Pt/C catalysts' surface using chronoamperometry for 1 h was analyzed by UV–visible spectroscopy and is

shown in Fig. 7a, b. During the electrooxidation of methanol, two stable by-products, i.e., formaldehyde and formic acid, were monitored. The absorbance vs concentration standard plots (data not shown) with a known concentration of formic acid and formaldehyde were obtained using UV–visible spectroscopy at the  $\lambda_{\text{max}}$  of 350 nm and 280 nm, respectively, for the estimation of MOR by-products. Figure 7a shows the absorbance spectra of the by-products and Fig. 7b shows that about 3% of methanol has been oxidized using PtCo (1:9)/rGO anode catalyst with 5 M methanol concentration and form formaldehyde and formic acid at room temperature, which is three times higher than that reported earlier ( $\sim 1\%$ ) using Pt black as anode material [34].

The performance of DMFC complete cell was tested for PtCo (1:9)/rGO and commercial Pt/C anode catalysts at varying temperatures and methanol concentrations. Figure 8a, b shows the cell voltage vs current density and power density vs current density curves for both the anode catalysts. The best half-cell performance by PtCo (1:9)/rGO was exhibited at 5 M methanol concentration. Therefore, 5 M methanol concentration was used with 3 mg/cm<sup>2</sup> anode catalyst loading with an operating temperature of 100 °C in a complete DMFC test. It could be seen in Fig. 9 that the power density from the single cell is almost the same (power density 22.66 mW/cm<sup>2</sup> at a current density of 52.0 mA/cm<sup>2</sup>) for PtCo (1:9)/rGO and commercial Pt/C anode catalysts in the low-current discharge region. The highest peak power density of 136.08 mW/cm<sup>2</sup> was observed for PtCo (1:9)/rGO which is  $\sim$ three times higher than that of highest peak power density (48.03 mW/cm<sup>2</sup>) of commercial Pt/C. Furthermore, PtCo (1:9)/rGO shows higher open-circuit voltage (OCV) as compared to the commercially available Pt/C, indicating that methanol crossover is less in the former case [35]. The cell performance, with different concentrations of methanol ranging from 1 to 5 M using PtCo (1:9)/

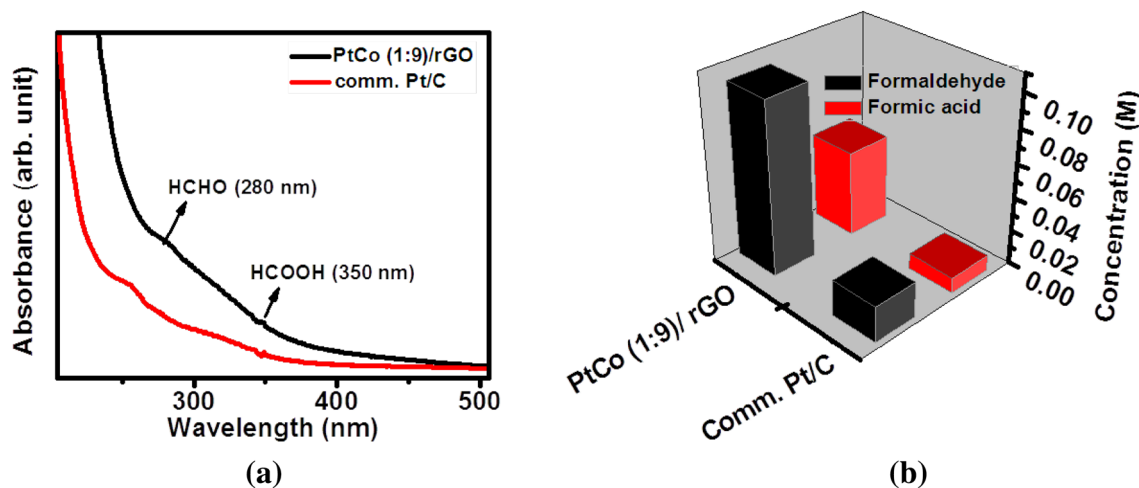


**Fig. 8** **a** UV–Vis absorption spectra of MOR by-products and **b** formation of formaldehyde and formic acid as a result of MOR at PtCo (1:9)/rGO with 5 M methanol



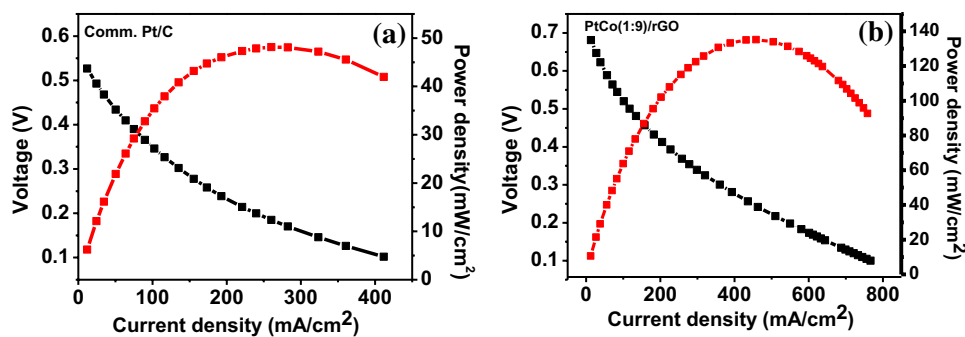


**Fig. 9** Electrical performances (cell voltage vs current density and power density vs current density) of a 5 cm<sup>2</sup> DMFC (3 mg/cm<sup>2</sup> catalyst loading).  $P_{O_2}$  = 1.5 bar; oxygen flow rate = 200, SCCM;

$P_{MeOH}$  = 1 bar; methanol flow rate = 1 mL/min; operating temperature = 100 °C electrolyte: Nafion 117 membrane **a** commercial Pt/C at 2 M methanol and **b** PtCo (1:9)/rGO at 5 M methanol concentration

**Table 1** Open-circuit voltage, current density, and maximum power density using PtCo (1:9)/rGO catalyst at different methanol concentration

Methanol concentration (M)	Open-circuit voltage (V)	Current density at 0.3 V (mA/cm <sup>2</sup> )	Current density at 0.4 V (mA/cm <sup>2</sup> )	Maximum power density (mW/cm <sup>2</sup> )
1	0.654	187.83	441.09	98.704
2	0.655	229.364	561.407	118.904
3	0.657	236.344	600.904	128.134
5	0.660	297.432	623.02	136.8

rGO as anode catalyst at 100 °C, in terms of variation in power density is illustrated in Fig. 9a and summarized in Table 1. The weak performance of DMFC at lower methanol concentration of 1 M is attributed to the mass transfer limitations, i.e., lack of optimum methanol availability at the electrode surface and anode kinetics remains unaffected [36]. Moreover, with increasing concentration of methanol, the MOR at electrode surface enhances which contributes towards higher power density.

Methanol electrooxidation on anode electrocatalyst in DMFC is a temperature-dependent process. The optimum-operating temperature for PtCo (1:9)/rGO was evaluated in direct methanol complete cell by varying the temperatures from 100 to 70 °C using 5 M methanol concentration and is shown in Fig. 9b. The power density linearly decreases from 136.8 to 93.7 mW/cm<sup>2</sup> when the operating temperature is decreased from 100 to 70 °C. A comparatively small difference in cell performance (power density) with a decrease in temperature from 80 to 70 °C suggests that the methanol crossover effect is significantly less at this temperature. In addition, OCV of the cell was observed to be almost independent of temperature. Furthermore, the low activation energy is favorable for the low operating temperature of DMFC and is dependent on the physicochemical properties such as the electronic structure of the alloy, particle size, and electrochemical behavior of support matrix of the catalyst [37]. To calculate the activation energy, considering various processes involved at electrode surface, the following relation has been considered [38]:

$$i = k \exp(\beta\theta_R) \exp\left(\frac{\beta'FE}{RT}\right), \quad (5)$$

where  $i$  is current density (measure of methanol oxidation rate),  $E$  is potential,  $\theta_R$  is the steady-state adsorption,  $\beta$  and  $\beta'$  are constants taken from literature [38],  $R$  is universal gas constants,  $T$  is absolute temperature, and  $F$  is Faraday constant. The reaction order is assumed to be 0.5, considering the reactions conditions similar to that reported by Khazova et al [38]. The steady-state adsorption  $\theta_R$  of methanol at real electrodes with carbon support is determined considering adsorbed intermediates CO and COH:

$$\theta = (\theta_{(H,CMeOH=0)} - \theta_{(H,MeOH)}) / \theta_{(H,CMeOH=0)}, \quad (6)$$

where  $\theta_{(H,MeOH=0)}$  and  $\theta_{(H,CMeOH=0)}$  are the reduction charge for hydrogen adsorption in the presence and absence of methanol, respectively. The model is assumed to obey Temkin equation:

$$\theta = a + (1/f) \ln c = a + (2.3/f) \log c, \quad (7)$$

where  $f$  reflects the distribution of adsorption site with respect to their adsorption energy and the value is taken as 23. The kinetics of methanol oxidation on real electrodes is assumed to obey Roginsky–Zeldovich equation:

$$V_{ads} = d\theta/dt = K_{ads} c \cdot \exp(-\alpha\theta), \quad (8)$$

where  $K_{ads}$  is the rate constant adsorption, and  $\alpha$  is the transfer coefficient taken as 1. Considering the above equations, steady-state adsorption rate,  $\theta_R$ , is calculated at 0.3 V,

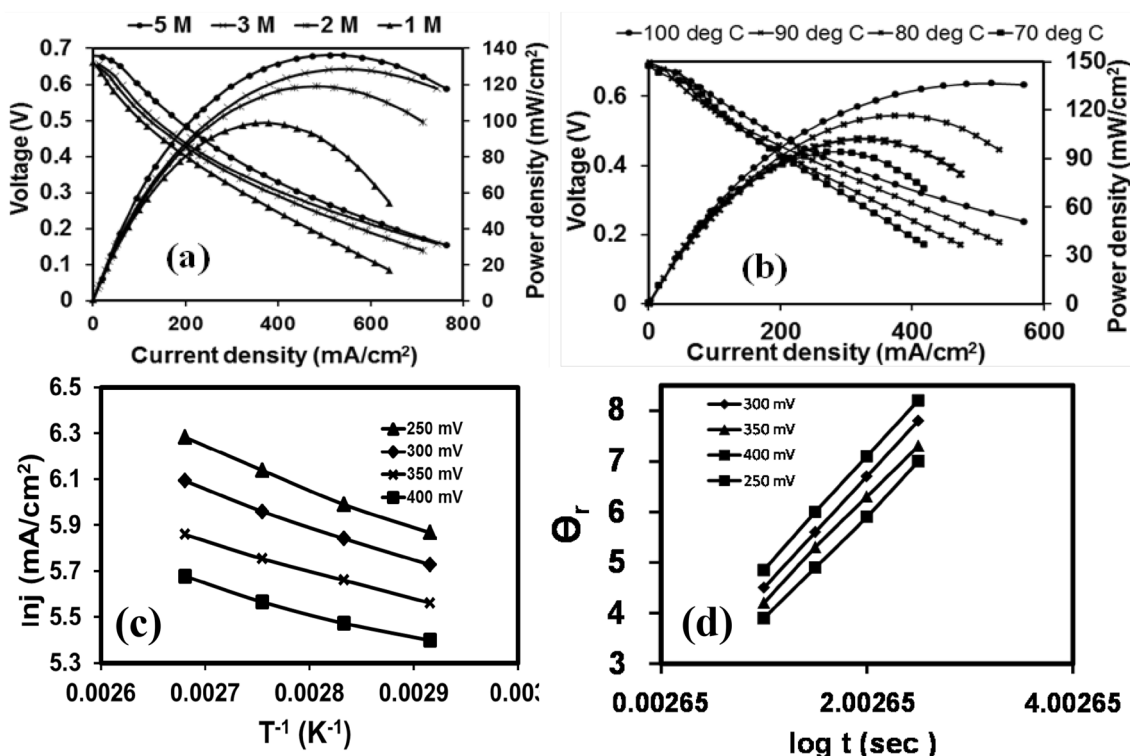


**Fig. 10** Electrical performances (cell voltage vs current density and power density vs current density) of a 5 cm<sup>2</sup> DMFC (3 mg/cm<sup>2</sup> catalyst loading).  $P_{O_2}$ =1.5 bar; oxygen flow rate=200, SCCM;  $P_{MeOH}$ =1 bar; methanol flow rate=1 mL/min; electrolyte: nafion 117 membrane **a** PtCo (1:9)/rGO performance at varying methanol con-

centration ranging from 1 to 5 M **b** PtCo (1:9)/rGO anode catalyst performance at varying temperature 100–70 °C using 5 M methanol concentration **c** Arrhenius plot of PtCo (1:9)/rGO at 250, 300, 350 and 400 mV potentials **d** kinetics of methanol adsorption on PtCo (1:9)/rGO

0.4 V, 0.5 V, and 0.6 V. The absolute current density has been calculated including methanol oxidation and ion transport parameters from equation (i) considering  $\theta_R$  at various potentials, and is shown in Fig. 10d and Table 2. The PtCo (1:9)/rGO, Arrhenius curves (logarithmic of current density versus temperature inverse) were generated at four different voltages (250 mV, 300 mV, 350 mV, and 400 mV) and at different operating temperatures, as shown in Fig. 10c. The linear decrease in activation energy is observed at a potential range of 250–400 mV and summarized in Table 2. The activation energy for PtCo (1:9)/rGO was calculated to be

**Table 2** Activation energy of PtCo (1:9)/rGO catalyst at different potentials

Voltage (mV)	Slope ( $\ln j/T_2^{-1} - T_1^{-1}$ )	$E_a$ (kJ/mol)
250	1733.8	14.41
300	1636.6	13.61
350	1188.4	9.88
400	1185.1	9.853

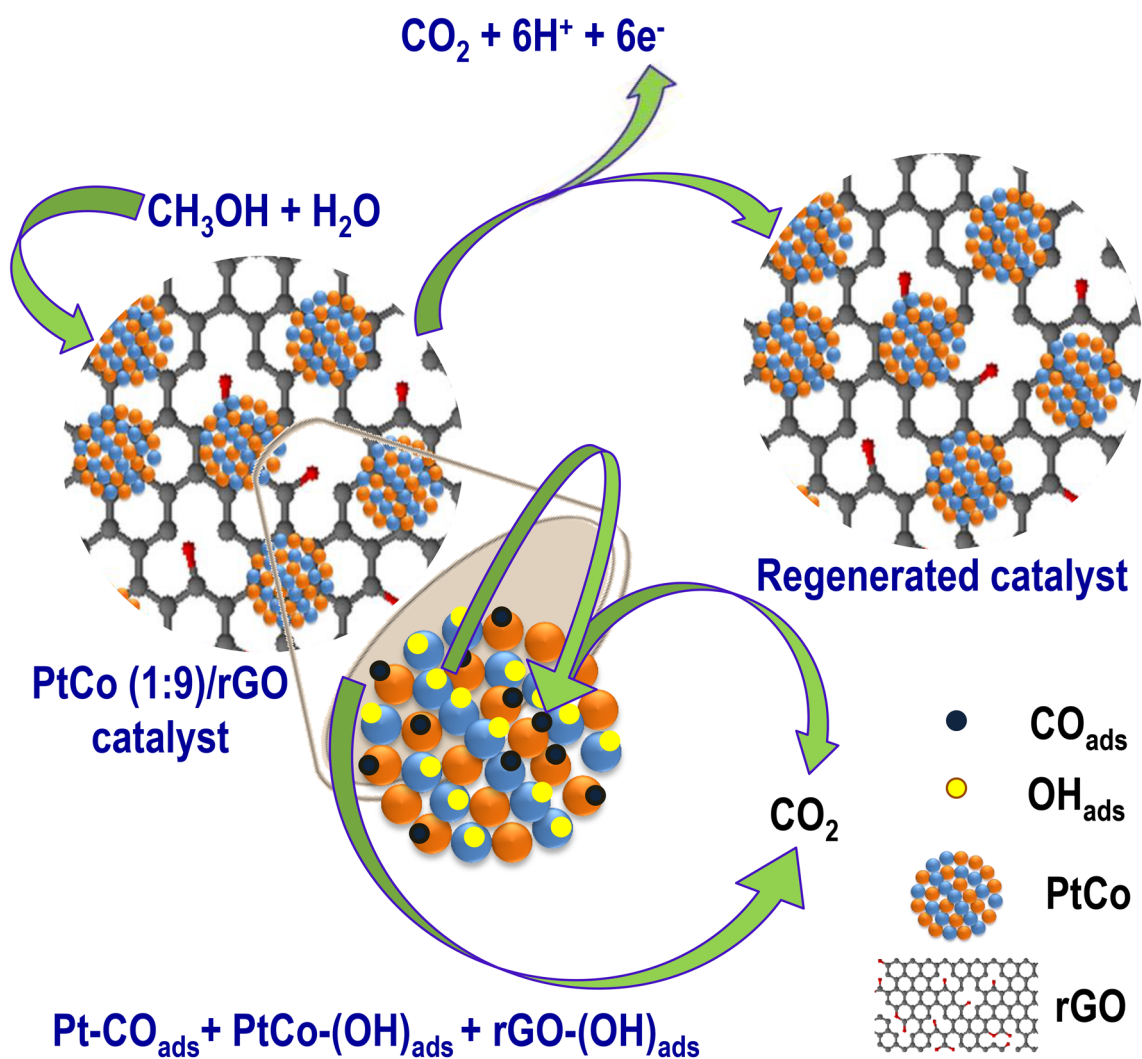
$J$  is current density with consideration of MOR and  $E_a$  is the value of activation energy after consideration of MOR

13.61 kJ/mol at 300 mV, and 9.88 kJ/mol at 400 mV, respectively, which is appreciably lower than that reported for Pt/C (70 kJ/mol) and PtRu/C (33.6 kJ/mol) which is considered more stable than Pt/C [39]. The comparison of presently synthesized PtCo (1:9)/rGO catalyst with recently reported anode catalyst on the basis of various operating parameters of DMFC is summarized in Table 3.

Putting together the above results, it is clear that the CO anti-poisoning behavior exhibited by the specific molar combination of Pt and Co in PtCo bimetallic nano-particles and hydrophilic nature of rGO plays a synergistic effect exhibiting high MOR activity and performance of DMFC. The schematic representation of synergistic electrode anti-poisoning mechanism is shown in Fig. 11. According to the bi-functional mechanism [12], addition of Co promotes the water activation, creating more OH<sup>-</sup> ions and other oxygen-containing species to oxidize CO like intermediates present on active Pt surface. The OH<sup>-</sup> ions also weaken the Pt–CO bond energy because of the charge transfer from Co to Pt, and thus, it creates a fresh Pt layer accessible for continuous electrooxidation of methanol and hence the catalytic activity. Furthermore, the synergy of PtCo nano-particles with oxygen containing functional groups of rGO support leads

**Table 3** Comparison of single cell DMFC parameters of PtCo (1:9)/rGO with the existing recent literature

S. no.	Anode catalyst	Methanol flow rate (sccm)	Oxygen flow rate (sccm)	Methanol concentration (M)	Temp. (°C)	Power density (mW/cm <sup>2</sup> )	Ref.
1	PtCoP/C (2016)	20	200	1	70	88.5	[40]
2	PtRu/MC (2013)	2	200	1	60	67	[41]
3	Au@Ag <sub>2</sub> S@Pt (2017)	1	300	10	80	89.7	[42]
4	N-GA/PtRu (2016)	–	–	0.5	90	93	[43]
5	Pt/Ce <sub>0.7</sub> Mo <sub>0.3</sub> /C (2016)	20	200	1	60	69.4	[44]
6	PtRuFe/NG (2017)	2	150	1	80	112	[45]
7	Pt@RFC (2017)	13.5	1000	1	80	87.2	[46]
8	PtRuMo/C (2014)	2		2	25	18.6	[47]
9	PtCo (1:9)/rGO (present work)	1	200	2	100	118.904	
				5	100	136.8	

**Fig. 11** Schematic representation of synergistic electrode antipoisoning mechanism

to the reduced electrode poisoning (Fig. S2a). The  $\pi$ - $\pi$  conjugation of  $sp^2$  hybridized carbon network present in rGO provides conducting paths for high electron transfer rate, thereby enhancing the electrode MOR kinetics and methanol oxidation efficiency. Hence, the electronic interaction between oxygen and PtCo atoms onto the rGO support collectively plays a key role in decreasing the adsorption of CO and efficient methanol oxidation.

## Conclusion

In summary, we have demonstrated the stability, higher methanol utilization efficiency, and MOR capabilities of PtCo (1:9)/rGO that are far superior to the commercially available Pt/C anode catalyst. The improved electrocatalytic properties of PtCo (1:9)/rGO anode catalyst for DMFC are attributed to the uniform and higher loading of small size PtCo nano-particles onto rGO surface. Furthermore, the synergy between the active surface of PtCo nano-particles as a result of favorable electronic structure and oxygen functional groups of rGO imparts enhanced antipoisoning characteristics to the electrode surface. The peak power density of  $136.8 \text{ mW/cm}^2$  at  $100 \text{ }^\circ\text{C}$  with  $5 \text{ M}$  methanol in complete DMFC test and activation energy of  $9.843 \text{ kJ/mol}$  suggests faster reaction kinetics of methanol oxidation for PtCo (1:9)/rGO anode catalyst and may be, for the first time, observed. The optimized DMFC operating parameters, high methanol utilization, and low activation energy of PtCo (1:9)/rGO anode catalyst indicate its commercial potential for real DMFC devices.

**Acknowledgements** The authors are grateful to the Director, CSIR-NPL for providing various research facilities to carry out the present work. SKS gratefully acknowledges Council of Scientific & Industrial Research, India, for funding under the project (P-81-103). SPS acknowledges NanoSHE (BSC0112). JG acknowledges the DST-INSPIRE (IFA-15/ENG107) for faculty funding and SERB-DST for the financial support (ECR/2017/000302). Authors are highly thankful to Professor S. Basu, IITD for extending his lab facility for methanol fuel cell testing, Mr. Dinesh Singh for TEM measurements and Mr. Sandeep Singh for AFM. RB gratefully acknowledges the financial support from P-81-103 and sincerely thank Shilpi Verma for technical discussions.

## Compliance with ethical standards

**Conflicts of interest** There are no conflicts to declare.

**Open Access** This article is distributed under the terms of the Creative Commons Attribution 4.0 International License (<http://creativecommons.org/licenses/by/4.0/>), which permits unrestricted use, distribution, and reproduction in any medium, provided you give appropriate credit to the original author(s) and the source, provide a link to the Creative Commons license, and indicate if changes were made.

## References

- Patil, M.B., Sapkal, V.S., Sapkal, R.S., Bhagat, S.L.: Direct methanol fuel cells—clean energy source for future. *Int. J. Res. Chem. Environ.* **2**, 7–12 (2012)
- Tiwari, J.N., Tiwari, R.N., Singh, G., Kim, K.S.: Recent progress in the development of anode and cathode catalyst for the direct methanol fuel cells. *Nano Energy* **2**, 553–578 (2013)
- Zenith, F., Na, Y., Krewer, U.: Optimal concentration control direct methanol fuel cells. *IFAC-PapersOnLine* **48**, 722–727 (2015). <https://doi.org/10.1016/j.ifacol.2015.09.054>
- Chakraborty, D., Bischoff, H., Chorrkendroff, I., Johansnessen, T.: Mixed phase Pt–Ru catalyst for direct methanol fuel cell anode by flame aerosol synthesis. *J. Electrochem. Soc.* **152**, 2357–2363 (2005)
- Burstein, G.T., Barnett, C.J., Kucernak, A.R., Williams, K.R.: Aspects of the anodic oxidation of methanol. *Catal. Today* **38**, 425–437 (1997)
- Kitchin, J.R., Norskov, J.K., Barteau, M.A., Chen, J.G.: Modification of the surface electronic and chemical properties of Pt (111) by subsurface 3d transition metals. *J. Chem. Phys.* **120**, 10240–10246 (2004)
- Xu, J.F., Liu, X., Chen, Y., Zhou, Y., Lu, T.H., Tang, Y.: Pt–Co alloy networks for methanol oxidation electrocatalysis. *J. Mater. Chem.* **22**, 236559–236567 (2012)
- Yaldagard, M., Jahanshahi, M., Seghatoleslami, N.: Carbonaceous nanostructured support materials for low temperature fuel cell electrocatalysts—a review. *J. Nano Sci. Eng.* **3**, 121–153 (2013)
- Geim, A.K., Novoselov, K.S.: The rise of graphene. *Nat. Mater.* **6**, 183–191 (2007)
- Gao, W., Alemany, L.B., Ajayan, P.M.: New insights into the structure and reduction of graphite oxide. *Nat. Chem.* **1**, 403–408 (2009)
- Ambrosi, A., Chua, C.K., Latiff, N.M., Loo, A.H., Wong, C.H.A., Eng, A.Y.S.: Graphene and its electrochemistry—an update. *Chem. Soc. Rev.* **45**, 2458–2493 (2016)
- Sharma, S., Ganguly, A., Papakonstantinou, P., Miao, X., Li, M., Hutchison, J.L., Delichatsios, M., Ukleja, S.: Rapid microwave synthesis of CO tolerant reduced graphene oxide supported platinum electrocatalyst for oxidation of methanol. *J. Phys. Chem.* **114**, 19459–19466 (2010)
- Wakisaka, M., Mitsui, S., Hirose, Y., Kawashima, K., Uchida, H.: Electronic structure of Pt–Co and Pt–Pu alloy for CO-tolerant anode catalyst polymer electrolyte fuel cell studied by EC-XPS. *J. Phys. Chem. B* **110**, 23489–23496 (2006)
- Kua, J., Goddard, W.A.: Oxidation of methanol on 2nd and 3rd row VIII transition metals (Pt, Ir, Os, Pd and Ru): application to direct methanol fuel cells. *J. Am. Chem. C* **121**, 10928–10941 (1999)
- Huang, H., Sun, D.P., Wang, X.: PtCo alloy nanoparticles supported on graphene nanosheets with high performance for methanol oxidation. *Chin. Sci. Bull.* **57**, 3071–3079 (2012)
- Jablonskiene, J., Kepeniene, V., Matusevičiūtė, A., Drabavičius, A., Tamašauskaitė-Tamasiunaite, L., Norkus, E.: Synthesis, characterization and properties of the graphene supported platinum–cobalt nanocatalysts. *Chemija* **26**(3), 159–164 (2015)
- Antolini, E., Salgado, J.R.C., Gonzalez, E.R.: The stability of Pt–M (M = first row transition metal) alloy catalysts and its effect on the activity in low temperature fuel cells. A literature review and tests on a Pt–Co catalyst. *J. Power Sources* **160**, 957–968 (2006)
- Baronia, R., Goel, J., Tiwari, S., Singh, P., Singh, D., Singh, S.P., Singhal, S.K.: Efficient electro-oxidation of methanol using PtCo

- nanocatalysts supported reduced graphene oxide matrix as anode for DMFC. *Int. J. Hydrog. Energy* **42**, 10238–10247 (2017)
19. Kovtyukhova, N.I., Ollivier, P.J., Martin, B.R., Mallouk, T.E., Chizhik, S.A., Buzaneva, E.V., Gorchinskiy, A.D.: Layer-by-layer assembly of ultrathin composite films from micron-sized graphite oxide sheets and polycations. *Chem. Mater.* **11**, 771–778 (1999)
  20. Song, S.Q., Liang, Z.X., Zhou, W.J., Sun, G.Q., Stergiopoulos, X.Q., Tsiakaras, P.: Direct methanol fuel cells: the effect of electrode fabrication procedure on MEAs structural properties and cell performance. *J. Power Sources* **145**, 495–501 (2005)
  21. Park, K.W., Sung, Y.E., Han, S., Yun, Y., Hyeon, T.: Origin of the enhanced catalytic activity of carbon nanocoil-supported PtRu alloy electrocatalysts. *J. Phys. Chem. B* **944**, 108939 (2004)
  22. Gao, H., He, L., Xiao, Y., Zhang, Y., Zhang, S.: One-step synthesis of reduced graphene oxide-supported PtCo nanoalloys with enhanced electrocatalytic activity for methanol oxidation. *Ionics* **22**, 2175–2182 (2016)
  23. Zhang, M., Shi, J., Ning, W., Hou, Z.: Reduced graphene oxide decorated with PtCo bimetallic nanoparticles: facile fabrication and application for base-free oxidation of glycerol. *Catalysis* **298**, 234–240 (2017)
  24. Verma, S., Singh, A., Shukla, A., Kaswan, J., Arora, K., Ramirez-Vick, J., Singh, P., Singh, S.P.: Anti-IL8/AuNPs-rGO/ITO as an immunosensing platform for noninvasive electrochemical detection of oral cancer. *ACS Appl. Mater. Interfaces* **9**, 27462–27474 (2017)
  25. Miller, D.J., Berg, H.O., Kaya, S.H., Casalongue, S., Friebel, D., Anniyev, T., Ogasawara, H., Bluhm, H., Pettersson, L.G.M., Nilsson, A.: Oxidation of Pt(111) under near-ambient conditions. *Phys Rev Lett* **107**, 195502 (2011)
  26. Fantauzzi, D., Calderin, S.K., Mueller, J.E., Grabau, M., Papp, C., Steinrck, H.P., Senftle, T., Jacob, P.: Growth of stable surface oxides on Pt(111) at near-ambient pressures. *Angew. Chem. Int. Ed.* **56**, 2594–2598 (2017)
  27. Vinayan, B.P., Rupali, N., Natarajan, R., Ramaprabhu, S.: Novel platinum–cobalt alloy nanoparticles dispersed on nitrogen-doped graphene as a cathode electrocatalyst for PEMFC applications. *Adv. Funct. Mater.* **22**, 3519–3526 (2012)
  28. Lu, J., Li, Y., Li, S., Jiang, S.P.: Self-assembled platinum nanoparticles on sulfonic acid grafted graphene as effective electrocatalysts for methanol oxidation in direct methanol fuel cells. *Sci. Rep.* **6**, 21530 (2016)
  29. Ren, F.F., Zhou, W., Du, Y., Yang, P., Wang, C., Xuc, J.: High efficient electrocatalytic oxidation of formic acid at Pt dispersed on porous poly(o-methoxyaniline). *Int. J. Hydrog. Energy* **36**, 6414–6421 (2011)
  30. Park, I.S., Park, K.W., Choi, J.H., Park, C.R., Sung, Y.E.: Electrocatalytic enhancement of methanol oxidation by graphite nanofibers with a high loading of PtRu alloy nanoparticles. *Carbon* **45**, 28–33 (2007)
  31. Liu, J.G., Zhao, T.S., Chen, R., Wong, C.W.: The effect of methanol concentration on the performance of a passive DMFC. *Electrochem. Commun.* **7**, 288–294 (2005)
  32. Li, L., Xing, Y.C.: Methanol electrooxidation on Pt–Ru alloy nanoparticles supported on carbon nanotubes. *Energies* **2**, 789–804 (2009)
  33. Kong, W.L., Masdar, M.S., Zainoodin, A.M.: Performances on direct liquid fuel cell in semi-passive and passive modes. *Am. J. Chem.* **5**(3A), 35–39 (2015)
  34. Liu, H., Song, C., Zhang, L., Zhang, J., Wang, H., Wilkinson, D.P.: A review of anode in direct methanol fuel cell. *J. Power Sources* **155**, 95–110 (2006)
  35. Parthiban, V., Akula, S., Peera, S.G., Islam, N., Sahu, A.K.: Proton conducting nafion–sulfonated graphene hybrid membranes for direct methanol fuel cells with reduced methanol crossover. *Energy Fuels* **30**, 725–734 (2016)
  36. Seo, S.H., Lee, C.S.: Effect of operating parameters on the direct methanol fuel cell using air or oxygen as an oxidant gas. *Energy Fuels* **22**, 1212–1219 (2008)
  37. Kauranen, P.S., Skou, E., Mink, J.: Kinetics of methanol oxidation on carbon-supported Pt and Pt + Ru catalysts. *J. Electroanal. Chem.* **404**, 1–13 (1996)
  38. Khazova, O.A., Mikhaiova, A.A., Skundin, A.M., Tuseeva, E.K., Havranek, A., Wippermann, K.: Kinetics of methanol oxidation on supported and unsupported Pt/Ru catalysts bonded to PEM. *Fuel Cell* **2**(2), 99–108 (2002)
  39. Zhanga, L., Cheng, X., Tua, H., You, M., Zhang, Y., Fan, Q.: Kinetic analysis of methanol oxidation on Pt/C and PtRu/C catalysts. *ECS Trans.* **11**, 1347–1357 (2007)
  40. Chang, J., Feng, L., Jiang, K., Xue, H., Cai, W.-B., Liu, C., Xing, W.: Pt–CoP/C as an alternative PtRu/C catalyst for direct methanol fuel cells. *J. Mater. Chem. A* **4**, 18607–18613 (2016)
  41. Bruno, M.M., Petrucelli, M.A., Viva, F.A., Corti, H.R.: Mesoporous carbon supported PtRu as anode catalyst for direct methanol fuel cell: polarization measurements and electrochemical impedance analysis of mass transport. *Int. J. Hydrog. Energy* **38**, 4116–4123 (2013)
  42. Feng, Y., Liu, H., Yang, J.: A selective electrocatalyst based direct methanol cell operated at high operated concentrations of methanol. *Sci. Adv.* **3**, 1700580–1700587 (2017)
  43. Zhao, S., Yin, H., Du, L., Yin, G., Tang, Z., Liu, S.: Three dimensional N-doped graphene/PtRu nanoparticle hybrids as high performance anode for direct methanol fuel cells. *J. Mater. Chem. A* **2**, 3719–3724 (2014)
  44. Zhang, G., Yang, Z., Zhang, W., Wang, Y.: Nanosized Mo-doped CeO<sub>2</sub> enhances the electrocatalytic properties of the Pt anode catalyst in direct methanol fuel cells. *J. Mater. Chem. A* **5**, 1481–1487 (2017)
  45. Li, K., Jin, Z., Ge, J., Liu, C., Xing, W.: Platinum nanoparticles partially-embedded into carbon sphere surfaces: a low metal-loading anode catalyst with superior performance for direct methanol fuel cells. *J. Mater. Chem. A* **5**, 19857–19865 (2017)
  46. Rethinasabapathy, M., Kang, S.M., Haldorai, Y., Jankiraman, M., Jonna, N., Choe, S.R., Huh, Y.S., Natesan, B.: Ternary PtRuFe nanoparticles supported N-doped graphene as an efficient bifunctional catalyst for methanol oxidation and oxygen reduction reactions. *Int. J. Hydrog. Energy* **42**, 30738–30749 (2017)
  47. Suo, C., Zhang, W., Shi, X., Ma, C.: Investigation of nano Pt and Pt-based alloys electrocatalysts for direct methanol fuel cells and their properties. *AIP Adv.* **4**, 031340–0313410 (2014)

**Publisher's Note** Springer Nature remains neutral with regard to jurisdictional claims in published maps and institutional affiliations.